ALIGNMENT AND DEFECT STRUCTURES IN ORIENTED PHOSPHATIDYLCHOLINE MULTILAYERS

SANFORD A. ASHER AND PETER S. PERSHAN, *Division of Applied Sciences, Gordon McKay Laboratory, Harvard University, Cambridge, Massachusetts 02138 U.S.A.*

ABSTRACT The alignment of dilauryl-, dimyristoyl-, and dipalmitoylphosphatidylcholine at various water concentrations into large oriented monodomain multilayers by annealing at elevated temperatures (Powers and Clark. 1975. *Proc. Natl. Acad. Sci. U.S.A.* **72**:840; Powers and Pershan. 1977. *Biophys. J.* **20**:137) is accompanied by the formation and subsequent dissolution of various defect structures. Some of these defects appear similar to those observed in thermotropic and other lyotropic liquid crystals, reflecting the lamellar structure of these materials. The formation and evolution of defects during the alignment of the lipids into the defect-free, monodomain, multilamellar geometry is studied using polarized microscopy. A combination of polarized and dark-field microscopy facilitated characterization of the defects; specific structural models are proposed. A new alignment technique involving compression and dilation of the lipid, which effects sample alignment at temperatures that are lower than those required by the Powers technique, is described. Lower temperature alignment avoids thermal decomposition that will sometimes occur if the lipid is maintained at elevated temperatures for prolonged periods. With this technique, samples (80 μm thick) of dilaurylphosphatidylcholine with 20% water by weight were aligned at room temperature.

INTRODUCTION

Recently Powers et al. (1–3) described an annealing technique for phosphatidylcholine-water mixtures that produces large (>125 μm thick × 1 cm^2 area) aligned monodomain multilayers. Aligned multilayers are of interest not only for their liquid crystalline properties (4–7) but also because of their utility as model systems in the study of biological membranes (8,9). In the latter context they can either be used directly for the study of the material properties of lipid bilayers (3,10–20) or as a matrix for the incorporation of biologically interesting ingredients (2,3).

In this article we will describe the use of polarized and dark-field microscopy to characterize the numerous defect structures (3) observed during the alignment of the lipid multilayers by both the annealing process of Powers et al. (1–3) and by a new alignment technique involving repeated compression and dilation of the sample. This new technique can be used to induce alignment of lipid liquid crystals at much lower temperatures than the annealing technique (1–3). This is significant because in the Powers technique the samples are annealed at temperatures that would denature many biologically interesting adducts, e.g., about 150°C for dipalmitoylphosphatidylcholine (DPPC) with 7% water by weight. In addition, the high annealing temperatures can lead to decomposition of the lipid if the sample is maintained at these high temperatures for prolonged periods. The Powers technique is also limited to lipid samples containing $< \sim 8\%$ water by weight (1,3); additional water could be

added after the sample was aligned. A combination of the mechanical alignment technique and the annealing technique permits the direct alignment of the lipids with any water concentration up to the two-phase limit.

Since the presence of defects can affect the results of many physical measurements, an understanding of their properties and the conditions for their appearance is a necessary prerequisite to careful studies. For example, material added to the multilayers often becomes selectively incorporated within some of the defects, leading to concentration inhomogeneities within the sample. Indeed, Wu et al. (14) noted selective incorporation of the fluorescent probe NBD-PE (N-4-nitrobenz-2-oxa-1,3-diazole phosphatidylethanolamine) within boundaries between oriented domains. The selective incorporation of fluorescent or spin-label probes into defects could result in diffusion and fluidity measurements characteristic of the defects rather than of the aligned multilamellar domains.

Although many of the defect structures appear spontaneously in freshly prepared samples, there are others that are only seen when well-aligned samples are subjected to thermal or elastic stresses (7). If one wishes to maintain well-aligned samples for any period of time it is essential to understand and control the conditions that lead to defect formation. Additionally, an understanding of the defect structures may elucidate the factors that prevent alignment and suggest improved alignment techniques. In this article we will describe the appearance of various lecithin samples during both the thermal annealing (1–3) and the mechanical alignment process. Some of these defects were observed earlier by Powers (3). Various defect structures will be identified and interpreted in terms of specific models.

EXPERIMENTAL

Dipalmitoyl- and dimyristoylphosphatidylcholine (DPPC and DMPC) were purchased from Sigma Chemical Co. (St. Louis, Mo.). Dilaurylphosphatidylcholine (DLPC) was purchased from Calbiochem (San Diego, Calif.) Our initial studies were with commercial DPPC samples that were chromotographed on silica gel columns (Bio-Rad Laboratories, Richmond, Calif., Bio. Sil. A, 200-400 mesh) using a chloroform methanol elution solvent. The lipid solution was rotary evaporated, leaving a waxy translucent solid, redissolved in benzene, and lyophilized into a fluffy powder. This powder was evacuated for 3 d at room temperature under <1.0 μm vacuum to ensure solvent removal. We subsequently discovered that if commercial lipids showing no TLC-detectable impurities were similarly lyophilized from benzene, they were experimentally indistinguishable from the chromatographed lipid in their alignment, defect structures, and phase transition temperatures. Most of the experiments reported here utilized the unchromatographed, TLC-pure commercial lipids. Benzene lyophilization appears to facilitate lipid alignment into the monodomain form and results in fewer defects. This may be because lipids dissolved in benzene have a high degree of local order (21). Recently we have observed that crystalline DPPC (Sigma Chemical Co., P6138) appears identical to the lyophilized lipids in its alignment, defect structures, and phase transition temperatures.

The lipid samples were monitored for purity by TLC on silica gel plates (EM Laboratories, Inc., Elmsford, N.Y., #5763) with an eluting solvent consisting of chloroform, methanol, and water (65:25:4 vol:vol). The plates were stained by iodine vapor and can detect as little as 0.5% lysolecithin. All three of the lipids were studied using the Powers technique (1–3) and were aligned between 1-mm thick microscope slides separated by a 125.0-μm teflon spacer. Samples containing $<10\%$ water by weight were prepared by adding the appropriate amount of water to the dry, lyophilized lipid power that had been packed into the cavity formed by the spacer and one microscope slide. A microliter syringe was used and the addition was carried out under dry nitrogen. The samples typically contained 10 mg of lipid. The top glass slide was then immediately pressed onto the sample and tightly clamped to prevent the escape of water during the annealing process. These samples were allowed to equilibrate overnight

before annealing. Water concentrations were measured gravimetrically for some of the lower water samples (<8%) subsequent to the annealing process. The water concentrations observed were within 10% of the values expected, indicating little loss of water during the annealing process for the lower water samples.

DPPC samples containing >10% water appear to require longer times for the water to become homogeneously distributed. To ensure water homogeneity, these samples were prepared in larger amounts (200 mg) by sealing the dry lipid powder with the appropriate amount of water in a glass vial under a N_2 atmosphere. The DPPC-water mixture was allowed to equilibrate at room temperature in the dark for 1 mo before use. No TLC-detectable lipid decomposition occurred during equilibration. Immediately after breaking the seal on the glass vial, about 10 mg of the lipid-water mixture was placed into the cavity formed by the spacer and the bottom microscope slide. The top slide was immediately clamped onto the sample. This procedure took <15 s and we presume that there was little exchange of water with the dry nitrogen atmosphere during the sample preparation.

Powers et al. (1–3) suggested that pretreatment of the glass slides by the silane surfactant N, N-dimethyl-N-octadecyl-3-aminopropyl-trimethoxy silyl chloride was essential for their alignment technique. However, we found that if the glass slides were scrupulously cleaned with hot chromic acid and then rinsed carefully in a distilled water steam bath, alignment was obtained equally well with or without the surfactant. On the other hand, the surfactant-treated surfaces are more convenient to use since they are both easily prepared and stable for weeks if stored under nitrogen. Clean surfaces are easily prepared since no water spotting occurs on the hydrophobic surfaces during the final rinse. In contrast, hydrophilic surfaces are easily contaminated even within a nitrogen atmosphere (presumably by trace organic impurities) and the surfaces become inhomogeneous. The hydrophilic surfaces must be used immediately after they are prepared. Most of our experiments were done with surfactant-coated slides.

The mechanical alignment of DLPC with 20% water was studied at room temperature. The samples were prepared by weighing the appropriate amount of water into a capsule containing 50 mg of dry lipid. The water was dispersed in the lipid using a dental amalgamator. Although the glass slides containing the samples were identical to those used in the annealing technique, the spacer was made of latex rubber, 100 μm thick. About 10 mg of the fluid lipid-water mixture was scraped out of the amalgamator capsule and placed into the cavity formed by the spacer and one glass slide. The second slide sealed the cavity and the entire assembly was placed into the holder shown in Fig. 1. The holder for the slides consists of a metal box and a steel plate that compresses the glass slides and rubber spacer together and against the bottom of the box. The tension on the steel plate was varied by set screws accessible from the top of the sample holder. Holes were drilled in the sample holder to monitor the alignment. Macroscopic alignment of DPLC containing 20% water could be obtained at room temperature (~25°C above T_c [8]) by gently alternating between compressing and releasing the glass slides. There was little or no bowing of the microscope slides during the compressions or dilations. In general, the compression was nonuniform, and flow from one part of the sample to another could be observed during the process. The flow may be

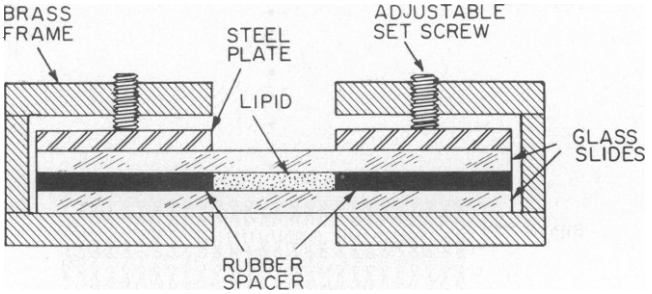

FIGURE 1 Sample holder for the mechanical alignment of lipids. Typical spacer thickness and lipid cross-sectional area are 100 μm and 1 cm^2, respectively.

partially responsible for the growth of the aligned homeotropic areas as the process is continued. The mechanical alignment technique can also be used to align any phosphatidylcholine-water mixture above the gel transition.

The alignment and defect structures were monitored continuously by using polarized optical microscopy and conoscopy. Defect-induced phase shifts in the transmitted light were measured at selected points in the sample by using a Soleil-Babinet compensator attached to the microscope.

RESULTS

Well aligned samples of DPPC, DMPC, and DLPC with various amounts of water (4–20%) at temperatures that correspond to their smectic-A or Lα phase are uniaxial (1–3, 16,20,22–25). The structure of these lipid liquid crystals has been shown by x-ray diffraction to consist of bilayers of lipid molecules separated by layers of water (Fig. 2) (1,16,20,22–27). Although there is a well-defined order along the normal to the layer planes, there appears to be no long-range order within the lipid layers (16,22–27). Since the optic axis of the homeotropically aligned lipid in the Lα phase is normal to the glass surfaces, a well-aligned sample appears uniformly dark when viewed between crossed polarizers. Defects in sample alignment, accompanied by tilts of the layers with respect to the glass slides, make the samples appear birefringent such that, when the plane of polarization of the incident light is neither parallel nor perpendicular to the tilt direction, the light leaving the sample will be elliptically polarized and will not be extinguished by a crossed polarizer. The magnitude of the effect is related to the amount of tilt, the magnitude of the uniaxial optical anisotropy of the aligned system, and the length of the tilted region as measured parallel to the direction of light propagation, i.e., normal to the glass slides. Thus, an unaligned lipid-water sample observed microscopically with white light between crossed polarizers appears to be nonuniform and highly colored due to the large variation of the layer tilts.

The phase diagrams of lecithin-water mixtures have been investigated by numerous groups (22–31). Hydrated DPPC samples containing >4 wt % water undergo a phase transition at

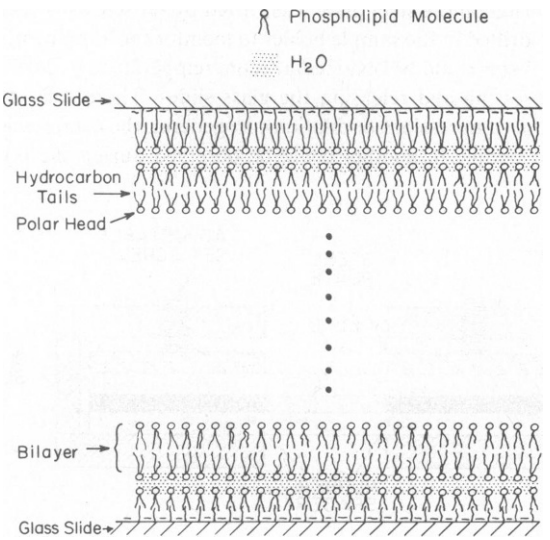

FIGURE 2 Schematic representation of the molecular geometry of lipid liquid crystals.

temperatures between 40 and 70°C (22,28) from a solid-like phase labeled L_β' in which the rigid hydrocarbon chains are tilted with respect to the bilayers (28) to an Lα or smectic-A phase where the hydrocarbon chains are fluid and perpendicular to the bilayers. The exact transition temperatures decrease with water content from ca. 65°C at 4 wt % water to 42°C at 20 wt % water.

Less is known about the high temperature (>100°C) hydrated-DPPC phase diagram, but from x-ray studies of egg lecithin (22,23,29,30) and soaps (32,33) it appears that cubic, hexagonal, and rhombohedral phases can occur where the lipid molecules are organized into rods (22,23,29,32,33). The cubic phase is unique in that it appears optically isotropic (29). Luzzati et al. (29) have shown that for egg lecithin containing <4 wt % water the rhombohedral phase occurs at ca. 70°C. This phase is followed by the cubic and hexagonal phases at about 90 and 120°C for samples containing <4 wt % water. However, Loomis et al. (30) indicate that egg lecithin samples containing <1 wt % water show a rectangular phase between 50 and 90°C followed by a cubic phase between 100 and 140° and a hexagonal phase between 140 and 240°C. In contrast, Small (23) indicated that the "viscous isotropic phase," which is cubic and optically isotropic, occurs at ca. 100°C for dry egg lecithin and appears at ca. 200°C for 16 wt % water. The phase transition temperature to the cubic isotropic phase increases with water content.

In our observations of DPPC samples containing 5–8% water, between room temperature

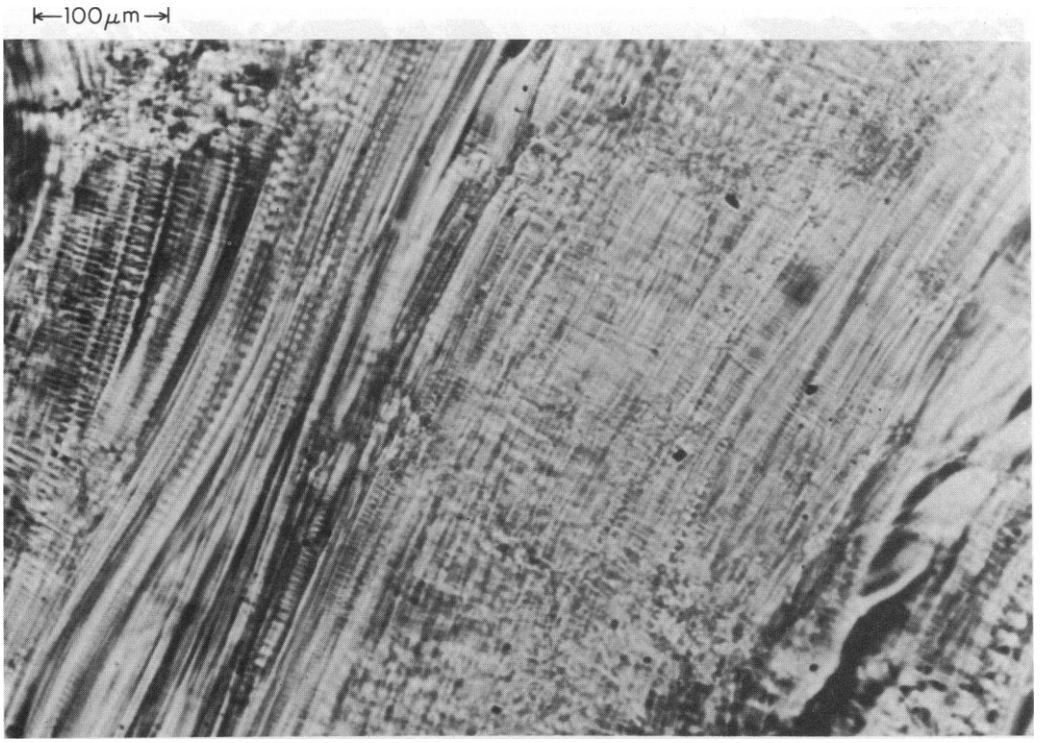

FIGURE 3 Striations along flow lines in a sample of DPPC with 7% water by weight. Sample thickness is 125 μm, T = 67°. The polarizers are oriented horizontally and vertically.

and 160°C, we observe the presence below ca. 70° of a solidlike birefringent phase (presumably L_{β}') that transforms at higher temperatures to a uniaxial phase containing defects indicative of the smectic-A or Lα phase. The magnitude of the optical uniaxiality of this phase decreases with temperature until a phase transition occurs to an optically isotropic phase we presume is cubic. At temperatures slightly below this transition to the optically isotropic phase (~5°C) defects begin to quickly anneal into a monodomain uniaxial geometry. Stresses on the sample will produce novel defects, which have not previously been identified with the smectic-A phase. These defects may indicate the presence of an additional phase between the Lα and the cubic phase or they may simply result from pretransitional effects that decrease the smectic elastic constants and permit new defect structures.

Thermal Annealing of Lipid-Water Mixtures

Figs. 3–6 contain typical views of different stages in alignment of a 125-μm thick sample of DPPC containing 7% water as observed microscopically between crossed polarizers. Dust spots that appear identical in some of these are on the microscope and not in the sample. At room temperature, which is well below the transition to the Lα phase, the sample appears brightly colored, amorphous, and featureless. Without polarizers it is waxy and translucent. As the temperature is increased, the sample apparently becomes more fluid, and at about 45°C inhomogeneous flow begins within the sample. Presumably this is the result of

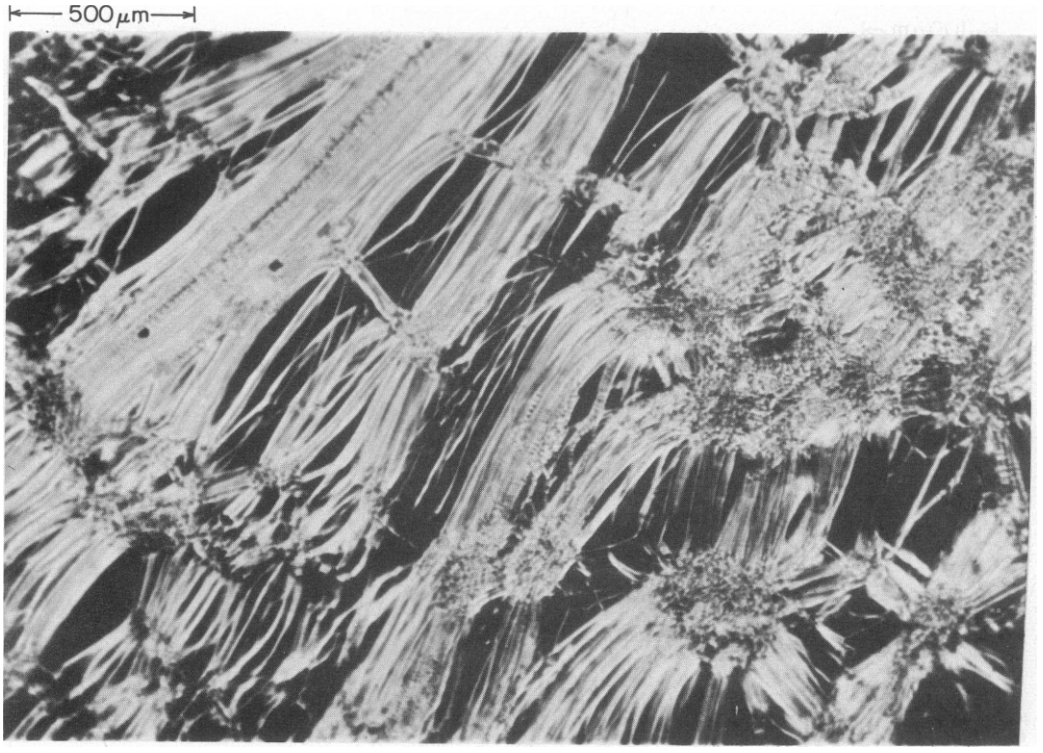

FIGURE 4 Oily streaks separating small black aligned domains in a 125-μm thick sample of DPPC with 7% water by weight. T = 77°C. The polarizers are oriented horizontally and vertically.

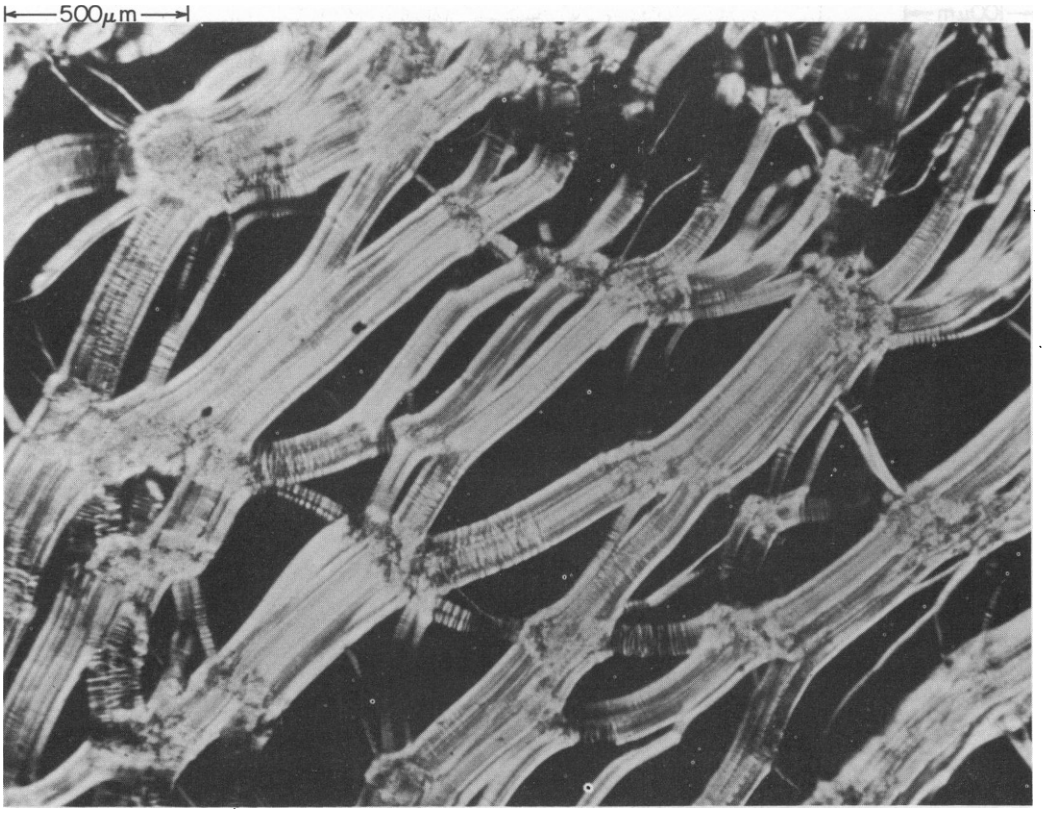

FIGURE 5 Oily streaks separating black aligned domains in 125-μm thick sample of DPPC with 7% water by weight. T = 83°C. The streaks connect at nodes. The polarizers are oriented horizontally and vertically.

inhomogeneous stresses produced when the sample was initially clamped between the glass slides. Fig. 3 shows the sample at 67°C. Striations, commonly referred to as "oily streaks" in the liquid crystal literature (3,6,30,34), can be observed. If these streaks are observed with white light and crossed polarizers, colored bands occur running parallel to some of the streaks. Additional structures, to be discussed later, can also be observed superimposed on the streaks. Fig. 4 shows a different section of the same sample at 77°C. Many of the streaks are separated off from the others and appear as isolated fine lines. Most of these are white or colorless. The wider streaks are white on the edge and sometimes become yellow, red, and even blue as one progresses into the interior. The black regions separating the streaks can be shown by conoscopy to be optically uniaxial, and we conclude that they are aligned regions with the lamella parallel to the glass surfaces. Fig. 5 also shows a different section of the same sample at 83°C. The aligned areas are larger and the streaks connect at nodes that appear to be pinned to the surfaces of the glass slides. Kleman et al. (6) pointed out that there appears to be a Kirchhoff's network relationship to the nodes; the width of an oily streak leaving a node is the sum of the widths of the oily streaks entering it. Although the widths of individual oily streaks appear to vary widely (1–300 μm), the wide streaks often seem to consist of thinner parallel streaks lying alongside each other. Forces causing flow in the sample transverse to the

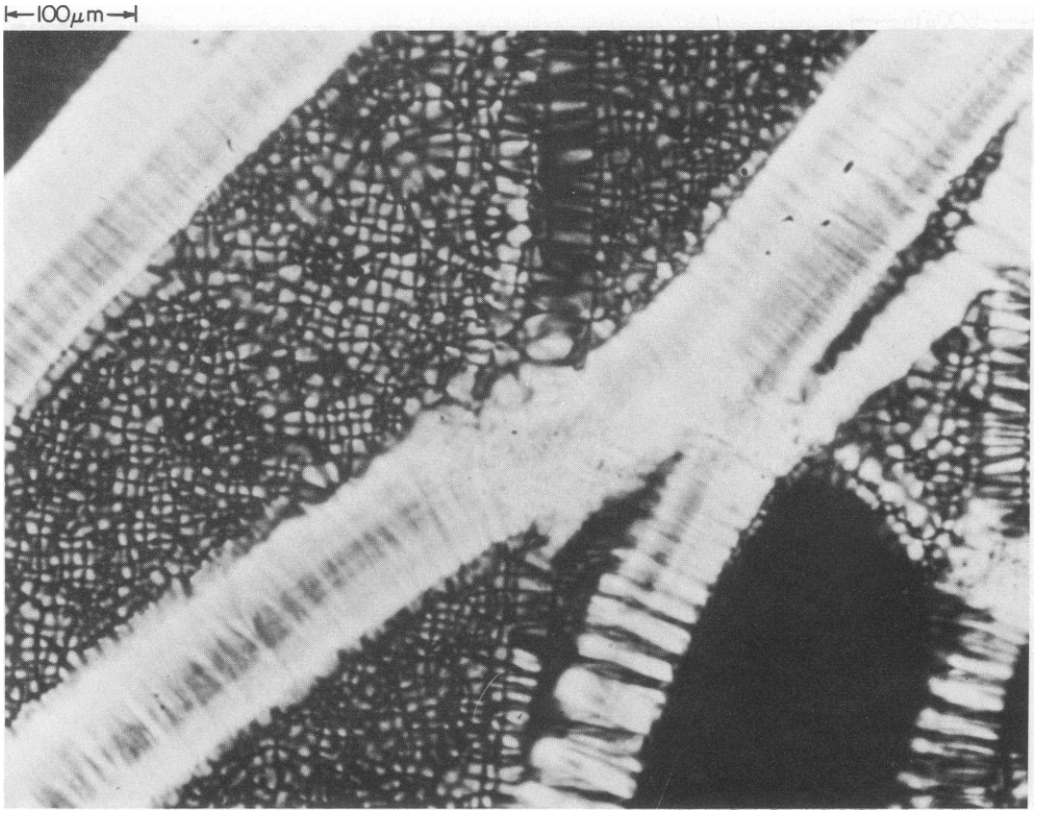

FIGURE 6 Polygonal array between oily streaks in 125-μm sample of DPPC with 7% water by weight. T = 110°C. Note the transverse black lines in the oily streaks connect to the black lines of the polygonal arrays. The polarizers are oriented horizontally and vertically.

streaks result in a separation of these parallel streaks. Impurities in the sample, such as dust and nonlipid soluble materials, tend to first become trapped in the streaks, and subsequently move along the streaks, finally collecting in the nodes. If smooth, unstructured oily streaks as those in Fig. 5 are viewed between crossed polarizers oriented parallel (perpendicular) to the long axes of the streaks, the light transmitted through the streaks is extinguished, indicating that the layer tilts are either along or perpendicular to the long axes. Observations using a Soleil-Babinet compensator indicate that the slow axis is perpendicular to the long axis of the streaks. Since the lipids are uniaxially positive (1–3) the layers must be tilted such that the layer normals remain perpendicular to the long axis of the streak. Observations of the colors transmitted through the crossed polarizers or measurements with a Soleil-Babinet compensator indicate that the maximum birefringence occurs at the center of an oily streak, decreasing almost symmetrically to either side. Although variations are observed in the maximum ellipticity of the transmitted light in different streaks, typically along the center of a streak 40 μm wide, the relative phase shift between light polarized parallel and perpendicular to the long axis corresponds to a path difference of ~600 nm. For wider oily streaks path differences as large as 1,000 nm have been observed.

The birefringence varies in a nonlinear manner across the oily streak. The rate of change is

perceptibly faster at the edge than at the center, where the birefringence is maximal. The oily streaks are well delineated from the adjacent aligned smectic domains, indicating that the layer tilts giving rise to the birefringence begin over a very short distance. In general, we find that the maximum birefringence for an oily streak increases with the width of the streak.

As the temperature is increased further, the aligned areas between the streaks continue to get larger and at about 100°C a polygonal defect array appears in all of the aligned areas. This is shown in Fig. 6 for the same sample as in the previous figures, but for temperature (T) = 100°C. These polygonal arrays are observed in all of the lipids studied and can also be formed in totally aligned samples by either small temperature increases or by slight increases in the spacing between the glass slides enclosing the sample (7). Similar polygonal arrays were observed by Powers (3) in DPPC and by Rosevear in soaps (34). Figs. 7 *a* and *b* show a crossed-polarizer and dark-field view of the polygonal array in a sample of DLPC containing 20% water by weight. This particular sample was aligned by the mechanical alignment technique and the polygonal array was formed by subjecting the sample to a small temperature increase (~2°C).

The polygonal arrays have been discussed at some length in a separate publication (7) and there is no need to reproduce the many observational details here. Suffice it to say that when they first appear, the polygonal arrays will look like a square grid of black lines for some orientations of the crossed polarizers with respect to the sample. For other orientations of the polarizer-analyzer combination, one still observed a square array, but with slightly different

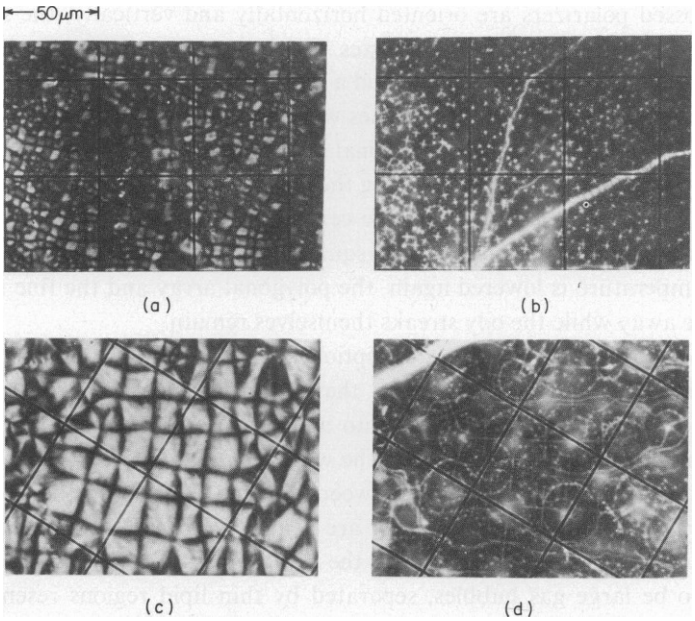

FIGURE 7 Crossed polarizer and dark-field photomicrographs of polygonal arrays. (*a*) Weakly birefringent polygonal arrays observed between crossed polarizers in a sample of DLPC containing 20% water by weight at room temperature. Focus is at the midheight of the sample. Reticule lines are 50 μm apart. (*b*) Same as (*a*), observed with dark-field microscopy. (*c*) Highly birefringent polygonal array observed between crossed polarizers in a sample of DLPC containing 20% water by weight at room temperature. Reticule lines are 50 μm apart. (*d*) Same as (*c*), observed with dark-field microscopy.

features. The appearance of the array also varies with the height at which the microscope is focused. Under dark-field illumination the array appears as small, fine, bright crosses in a uniformly dark field (Fig. 7 *b*). The position of the crosses correlate with certain vertices in the grid pattern observed between crossed polarizers. Although the polygonal array is stable for many hours if the temperature and sample thickness are held fixed, it will disappear in a matter of seconds if the temperature is lowered a few degrees or if the glass plates enclosing the sample are slightly compressed.

The polygonal array that first appears is essentially colorless even though the oily streaks may be brightly colored. With further increases in the temperature or larger sample dilations the polygonal array becomes coarser (the period increases by a factor of two or three) and more birefringent, acquiring a yellow hue. Furthermore, for the initial array, when the polarizer-analyzer combination was parallel to the grid lines, the spaces between the lines were uniformly gray. For the new array there is definitely some structure. This is most strikingly seen in Fig. 7, where the crossed-polarizer and dark-field views of the two arrays are compared. The birefringent polygonal array shown in Figs. 7 *c* and *d* is taken from a different section of the same sample, as shown in Figs. 7 *a* and *b*, and was formed by a dilation of the sample ($\sim 10\ \mu m$).

When the polygonal arrays form upon a temperature increase or a sample dilation, fine structure forms within the oily streaks transverse to their long axes. This transverse structure is most pronounced when the crossed polarizers are oriented either parallel or perpendicular to the streaks and can be clearly seen in the several streaks shown in Fig. 6.

Since the crossed polarizers are oriented horizontally and vertically, the streaks that are most visible are those running 45° to these axes. On the other hand, it is possible to identify a faint vertical streak in the center of Fig. 6, and a slightly more evident one on the very right. If the polarizer were rotated 45°, the bright ones would become faint and the faint ones bright. Since the dark lines that make up the polygonal array run into the streaks, it is often difficult to distinguish between a streak oriented along the polarizer analyzer axis and the surrounding array. In this figure the vertical streak in the center can only be identified by comparing the horizontal dark and light bands with the square pattern characteristic of the array. If, however, the temperature is lowered again, the polygonal array and the fine structure in the oily streaks fade away while the oily streaks themselves remain.

Although there is not a precise description of the DPPC-water phase diagram at temperatures above ~110°C, it is known that above this temperature the system can transform for some water concentrations into a "cubic isotropic" phase (8,22,23,28). The actual transition temperature is sensitive to the water content and sample purity (22,23) (see below) and in our experiments it varies between 110 and 160°C. On the other hand, when samples containing more than 8–10% water are heated to ~125°C it appears as though the vapor pressure of water in equilibrium with the sample rises precipitously. Fig. 8 illustrates what appears to be large gas bubbles, separated by thin lipid regions resembling myelinic figures. Under these conditions the gas, which we presume to be water vapor, is of sufficient pressure to force the glass slides to separate from the spacer and the lipid to flow out of the sample. This is the reason why the Powers alignment technique is restricted to samples containing <8–10% water, and why the sample holders that Chapman used for his differential scanning calorimetry studies of DPPC burst at high temperatures (22). Due to sample

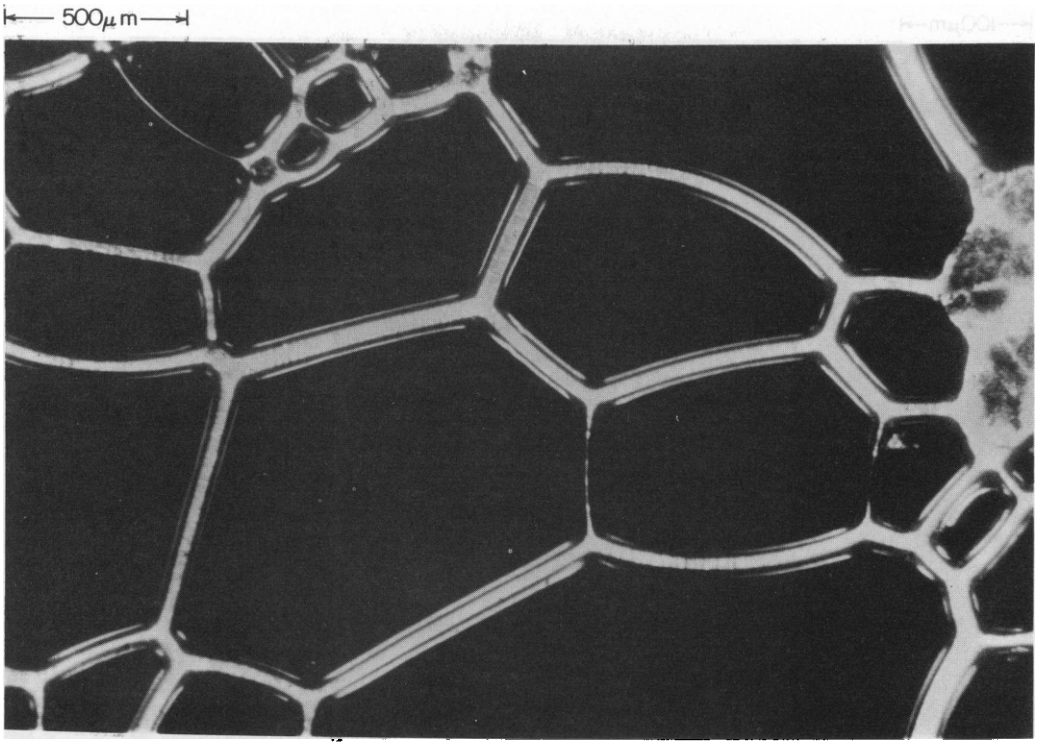

FIGURE 8 Myelinic figures separating bubbles of steam in a 125-μm thick DPPC sample containing 20% water by weight. T = 135°C.

disruption by steam formation we were unable to investigate lipid-water phases occurring above 125°C for water concentrations above 10 wt %.

With samples containing <8–10% water, if the temperature is raised to within 5°C of the transition to the cubic isotropic phase, the polygonal array will fade away in times of order of minutes. The polygonal array starts to anneal at those sites that display crosses under dark-field illumination. This is easily seen when viewed between crossed polarizers, since the regions surrounding the crosses darken noticeably and the dark lines emanating from these sites broaden until the entire array disappears. Accompanying this process is a decrease in the birefringence of the unannealed portions of the array. Fig. 9, showing a polygonal array in the process of annealing away at 128°C, demonstrates the sharp contrast that occurs between the annealed sections of the array and those parts that have not yet annealed away. The defect texture in Fig. 9 superficially resembles textures observed by Rosevear (34) in the middle phases of soaps. However, the texture in Fig. 9 results from an annealing of the polygonal array formed within the $L\alpha$ phase into a planar uniaxial domain and is not a stable defect texture at this temperature. Thus, the new texture observed at this temperature cannot be used to diagnose the presence of a new phase in lipids similar to the middle phase of soaps.

The oily streaks are the last features to disappear, and one is left with a uniformly aligned sample that is black between crossed polarizers, except for a few isolated pointlike defects. Conoscopy indicates that although the sample is uniaxial, the optical anisotrophy, Δn, at these

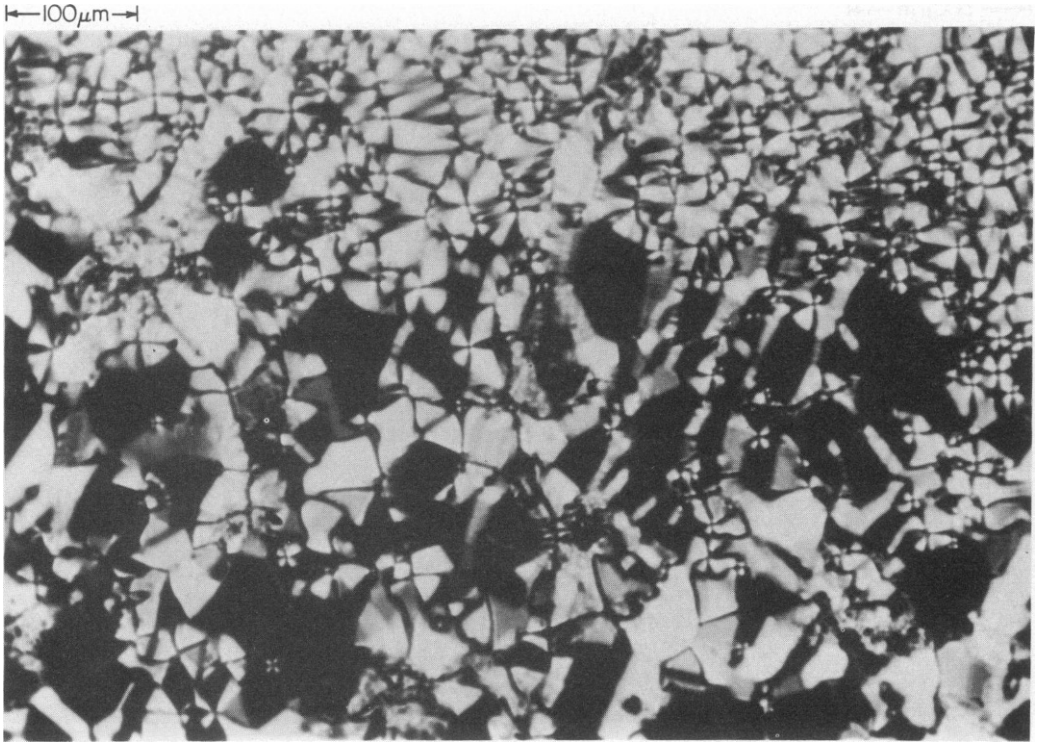

FIGURE 9 Polygonal arrays and oily streaks annealing away in a 125-μm thick sample of DPPC containing 7% water by weight. T = 128°C.

temperatures is much smaller than the values measured at lower temperatures (1–3) (i.e., $\Delta n \ll 0.01$). Note that the gradual annealing of the polygonal arrays at temperatures slightly below the optically isotropic phase is qualitatively different from the dissolution that occurs at lower temperatures, simultaneously with a decrease in sample temperature.

If the sample temperature is lowered slowly, a well-aligned, defect-free sample will be maintained and Δn becomes ~0.03 at 80°C (1–3). If, however, the temperature is lowered too quickly (i.e., faster than 1°C/min), thin strandlike defects appear that run between the point defects that remained in the aligned sample (Fig. 10). These strands will eventually anneal away at any temperature within the Lα phase. Slow cooling will maintain an aligned defect-free sample down to the gel transition temperature. If the aligned sample is stabilized at some temperature above the gel transition but more than ~5°C below the high temperature transition to the optically isotropic phase, small increases in sample temperature (~0.1°C) or small increases in sample thickness will immediately induce the polygonal array mentioned above. Reversal of the temperature or thickness increase causes the array to completely vanish. If the aligned sample is maintained at a temperature no more than ~5°C below the transition to the optically isotropic phase, the polygonal array will not appear under any conditions.

If the sample is cooled below the gel transition temperature, defects commonly occur in the sample alignment. These defects appear as numerous diffuse regions scattered throughout the

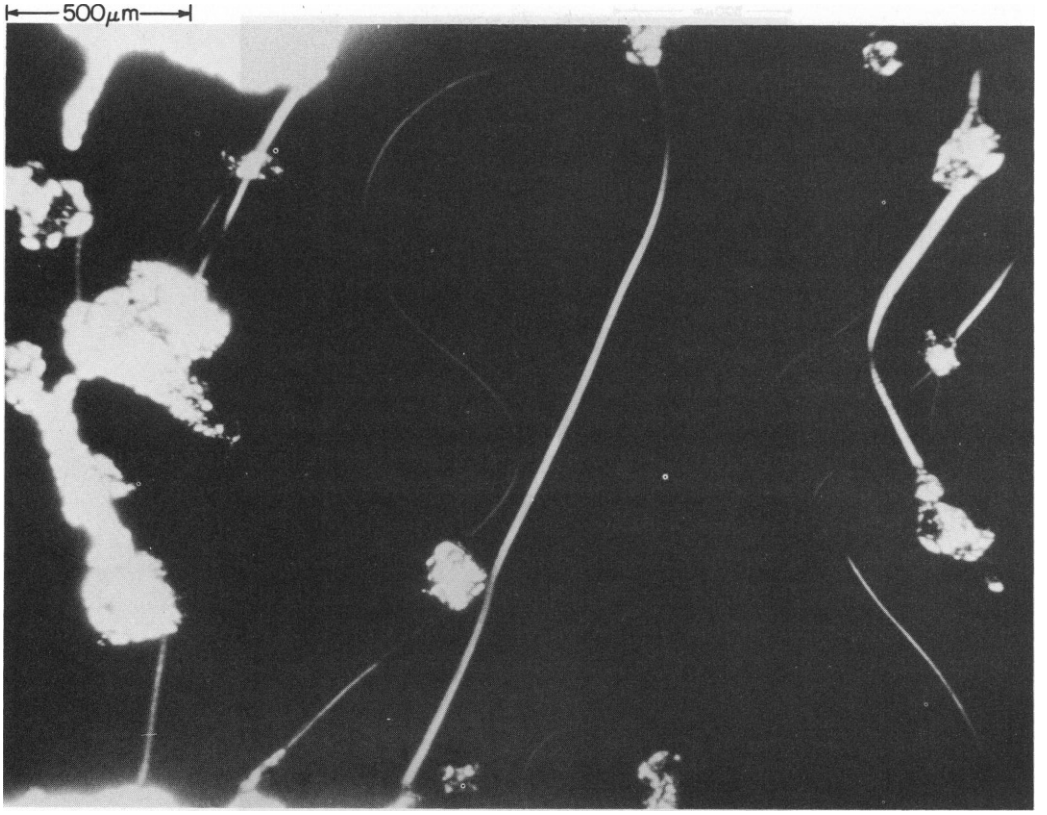

FIGURE 10 Strandlike defects formed in aligned domains by a fast temperature decrease. The strands connect defects in the 125-μm thick sample of DPPC containing 7% water by weight. The temperature was lowered from 130°C to 122°C in ~ 1 min.

sample that transmit light through the crossed polarizers. Even for samples that appear macroscopically-oriented by conoscopy, microscopic observations will often indicate that the alignment is far from perfect.

The transition to the optically isotropic phase can be monitored microscopically, since even after the polygonal arrays anneal away, ~5° below the transition, the sample does not appear totally black. Presumably, some light is transmitted through the crossed polarizers due to small deviations in the alignment of the sample. The onset of the isotropic phase is indicated by the appearance of a totally black area containing almost no defects. A definite border between the optically isotropic phase and the rest of the sample can be observed by using natural illumination. If the entire sample becomes isotropic, the planar uniaxial phase can never be recovered and subsequent cooling results in the needle-like structures shown in Figs. 11 *a* and *b*. However, if the sample is prevented from becoming completely isotropic by quickly lowering the temperature a few degrees at the first appearance of the isotropic phase, the sample appears as an inhomogeneous mixture of needle-like and planar domains. If the temperature of the sample is maintained no more than ~5°C below the isotropic transition, the needle-like domains slowly dissolve into the planar regions. We observe transitions to an optically isotropic phase for lipids containing between 3 and 8 wt % water.

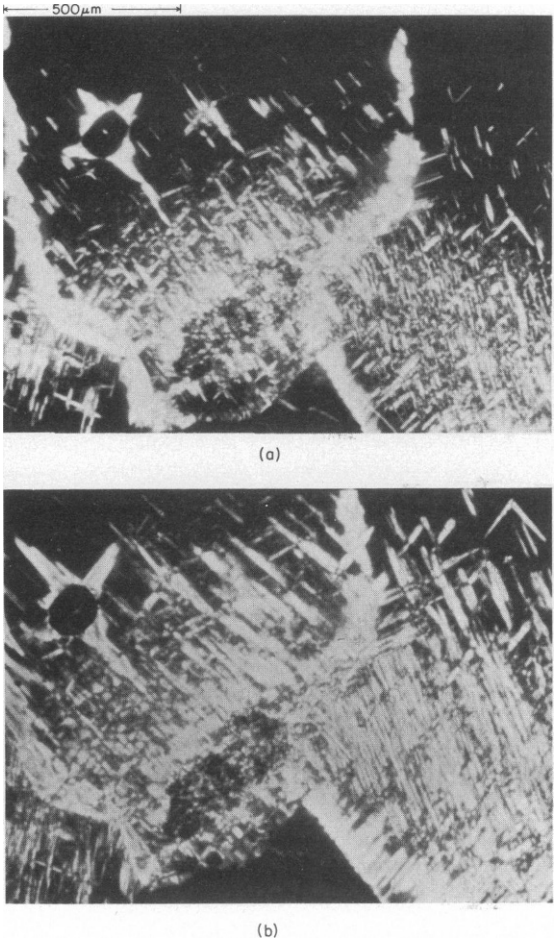

FIGURE 11 Needle-like defects formed upon a temperature decrease from the isotropic phase in a 125-μm thick DPPC sample containing 7% water. (*a*) T = 148°C. (*b*) T = 145°C.

In all of the DPPC samples that we have studied carefully, the isotropic phase transition decreases with time if the samples are maintained at elevated temperatures (>100°C) for prolonged periods. For example, a fresh DPPC sample containing 7% water by weight will initially show an isotropic transition temperature at about 160°C. However, if the sample is maintained at 115°C, the transition temperature will steadily fall and after about 1 wk will become optically isotropic at 115°C. This decrease in the transition temperature is not due to water loss, since subsequent measurements of the water concentration agree with the expected water content. However, the decrease in the isotropic transition temperature can be correlated with the appearance of palmitic acid, lysolecithin, and other unidentified products that can be detected by TLC. Their concentration increases with time from what we estimate to be ~1% after 4 h at 150°C to ~50% after 1 wk at 150°C. Although thermal decomposition of unsaturated lipids is well known, there is little published information on saturated lecithins except for the observation of thermal decomposition at 210°C (22).

The rate of lipid decomposition is a function of both the temperature and water content.

The rate of decomposition is slowest in monohydrate samples; after 2 d at 150°C the intensity of the lysolecithin spot on the TLC plate corresponds to that of a fresh lipid sample intentionally mixed with 5 wt % lysolecithin. The amount of lysolecithin in monohydrate samples maintained at 90°C for 2 d is below the limit of detection (<0.5%). In contrast, although 7% water samples maintained at 150°C for 2 d are severely degraded (~50%), one can barely detect any lysolecithin in 7% water samples maintained at 90°C for 2 d. This corresponds to <~0.5 wt %. A 25% water sample shows about a 2% decomposition after 2 d at 90°C. These results indicate that any lipid-water sample should be annealed for a minimum time above 100°C.

The defect structures observed in these lipid-water samples appear almost independent of sample purity for samples containing <~10 wt % of degradation products. The major effect of degradation that we observe is a lowering of the isotropic transition temperature (22,23). More severely degraded samples do not align into homogeneous domains and have numerous defects. Interestingly, for those samples most severely degraded, the textures observed under the optical microscope suggest that they are aligned with the layers perpendicular to the glass slides.

As previously mentioned, the polygonal array will only form at temperatures that are >~5°C below the isotropic transition temperature. However, if the sample is <5°C below that transition, a new series of defect structures can be formed, either by dilating or compressing the sample. The first of these appears at temperatures just above the temperature where the polygonal array anneals away. This structure might also be described as polygonal, although its appearance is qualitatively different from the appearance of the array that was previously termed polygonal; e.g., compare Figs. 6 and 12. The structure often consists of short parallel

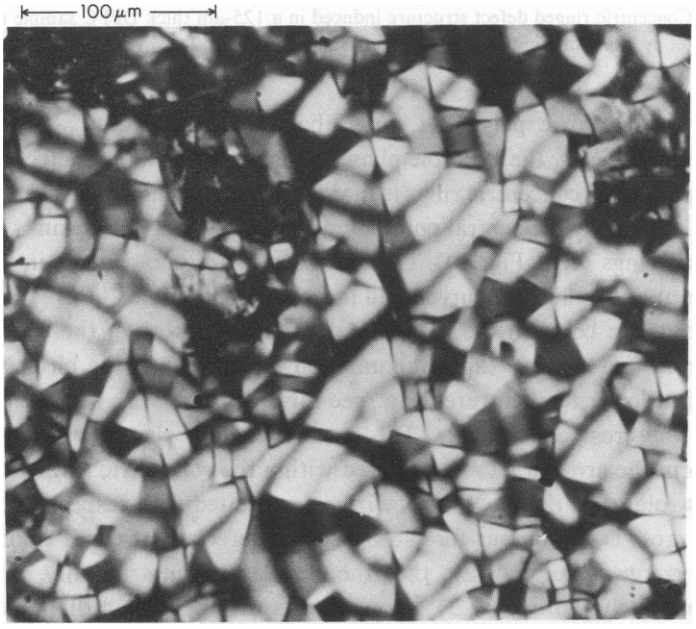

FIGURE 12 Second polygonal defect structure induced in a 125-μm thick DPPC sample containing 7% water by weight by squeezing and releasing glass slides. ~5°C below the isotropic transition temperature.

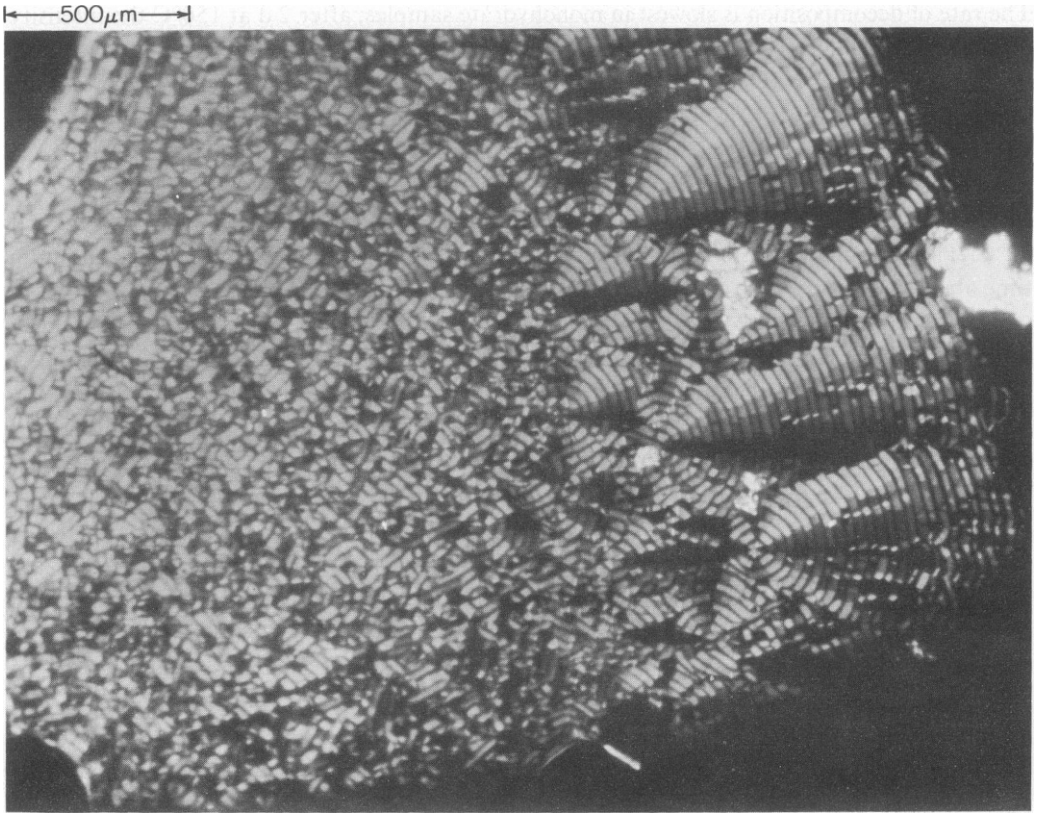

FIGURE 13 Concentric ringed defect structure induced in a 125-μm thick DPPC sample containing 7% water by weight by either dilating or compressing the sample. T = 150°C.

bands that form concentric polygonal rings about a central point. At a slightly higher temperature, but still below the isotropic phase, a somewhat different defect structure occurs (Fig. 13). The pattern of concentric rings is more pronounced and extensive than those in Fig. 12, and the structure near the central point is smooth, displaying fewer kinks in the curvature of the concentric rings (e.g., Fig. 14). On the other hand, one can see in Fig. 13 that the concentric rings are not smoothly curved and facets are still visible.

The repeat distance between the light and dark rings of both of these defects is roughly constant and from two to three times the unit cell dimensions of the birefringent polygonal arrays observed at lower temperatures (e.g., see Fig. 7 *c*). The dark rings remain dark for all orientations of the crossed polarizers. The concentric light rings have superimposed dark sections that form the arms of a cross centered within the concentric rings (Figs. 13 and 14). This dark cross rotates as the crossed polarizers are rotated with respect to the sample. The rotation of the cross is continuous for those circular defects that curve smoothly. Measurements using a compensator indicate that the slow axis points radially. Since the optical anisotropy is uniaxially positive (1–3), the layer tilts must also be radial. The more angular defect structures (Fig. 12) appear to be composed of connecting segments that are dark when they are oriented along the crossed-polarizer axes; e.g., light is extinguished in a segment

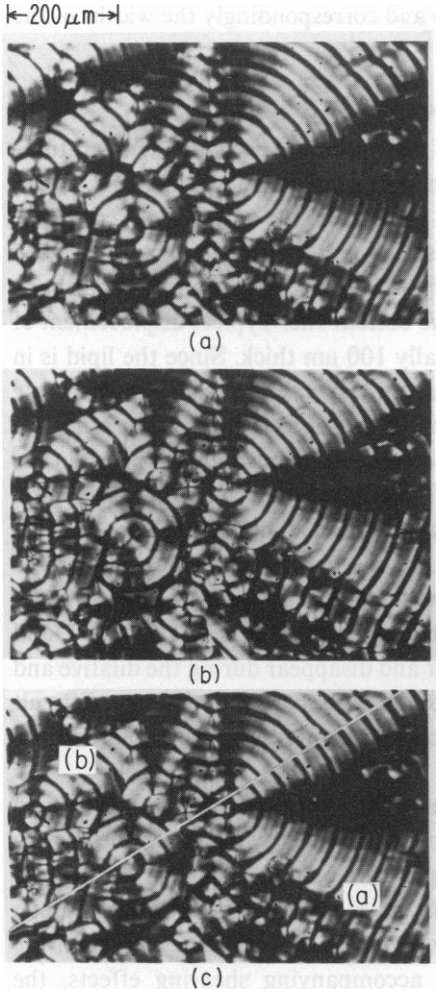

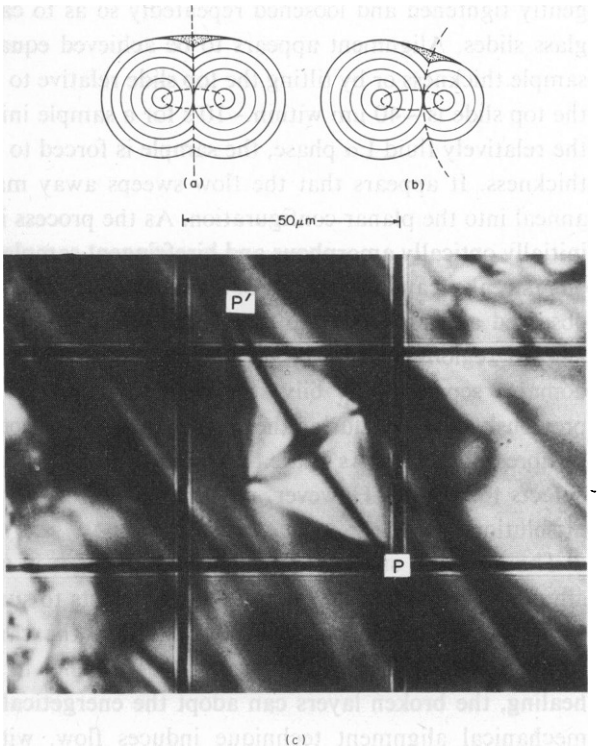

FIGURE 14

FIGURE 15

FIGURE 14 Closeup of the defect structure shown in Fig. 13 with the microscope focused (*a*) at the top of the sample, and (*b*) at the bottom of the sample. The complementary nature of parts (*a*) and (*b*) are illustrated in the composite (*c*).

FIGURE 15 (*a*) Layer curvatures in a focal conic consisting of a line and circle pair. (*b*) Layer curvatures in a focal conic consisting of an ellipse and hyperbola. (*c*) Focal conic observed in a 100-μm thick DLPC sample containing 20% cholesterol. T = 60°C.

when the segment's outer edge is along the polarizer axes. As the crossed polarizers are rotated, a segment that is dark becomes light while the adjacent light segment becomes dark. The direction of the optic axis appears to change discontinuously between segments.

The maximal contrast between the light and dark rings in these defects is observed when the microscope is focused at either the top or bottom of the sample (Fig. 14). Those black rings observed at one height are out of focus at the other, and are replaced by a new set of black rings centered within the original light rings. None of the black rings are in focus within the sample. The defect structures shown in Figs. 12–14 are stable for only a few minutes. As

they anneal away the widths of the black rings increase and correspondingly the widths of the light rings decrease.

Mechanical Alignment of Lipid Water Mixtures

Aligned lipid-water samples can be prepared far below their isotropic transition temperatures but above their gel transition temperatures by using the sample holder shown in Fig. 1. While observing the sample microscopically between crossed polarizers, the various set screws are gently tightened and loosened repeatedly so as to cause the material to flow parallel to the glass slides. Alignment appears to be achieved equally well by either a uniform change in sample thickness or by tilting the top slide relative to the bottom one. Typical displacement of the top slide is ~40 μm within ~10 s for a sample initially 100 μm thick. Since the lipid is in the relatively fluid Lα phase, the sample is forced to flow in response to the changing sample thickness. It appears that the flow sweeps away many of the defects and forces others to anneal into the planar configuration. As the process is continued, aligned areas appear in the initially optically amorphous and birefringent sample. The aligned regions become larger and oily streaks can eventually be identified separating the aligned domains. The textures observed appear similar to those shown in Figs. 4–6. As the process continues further the aligned regions become larger and larger until the entire sample consists of aligned black domains separated by oily streaks. The polygonal textures shown in Figs. 6 and 7 and previously observed during the annealing process appear and disappear during the dilative and compressive stages. As in the thermal annealing process, the oily streaks are the most difficult defects to remove. However, repeated cycles of dilation and compression slowly force their dissolution.

The flow and stresses resulting from changes in sample thickness during the mechanical alignment technique presumably allow defects to surmount the energy barriers necessary to form aligned domains. Dislocations within the sample can be squeezed out during the compressive stages (35) and layers not parallel to the glass slides may be broken. Upon healing, the broken layers can adopt the energetically favorable planar form. Although the mechanical alignment technique induces flow, with accompanying shearing effects, the conceptual difference between it and the shear alignment technique (3,4,18) can be seen by considering the idealized case of a sample with no defects and perfectly flat, parallel glass slides. Squeezing such a sample will only cause flow if individual layers can break, to form some sort of dislocation loop or similar defect. In that case the loop is unstable and flow occurs to relieve the built-up stress. At the end of the process such an idealized sample would be restored to the original state, except for being slightly thinner. In real samples, squeezing will cause the pre-existing dislocations and defects to move at stresses below (35) the values that would cause new defects. The primary action of the mechanical technique is thus to develop conditions under which motion of the defects out of the sample would relieve the static stress. In contrast, for the idealized perfect sample, the shear technique would produce a homogeneous velocity gradient that may or may not be stable for practical shear rates. If, for argument's sake, we assume the flow is stable in the ideal sample, the expected effect of defects on the flow, or conversely, the expected effect of flow on the defects, is less obvious. One possible picture would have the lipid flow so as to avoid the defects. Presumably, this would have a back reaction on the defect that will cause it to move out of the sample in some manner. Without an elaborate theoretical study further speculations of this type appear futile.

The empirical facts are that both techniques will result in alignment. However, we have found that the mechanical technique results in thicker aligned samples than the shear technique (~100 μm compared to ~20–50 μm). Although for both techniques polygonal arrays occur during the aligning process, they are easily removed in the mechanical technique by readjusting the sample thickness. As a practical matter, if the shear technique was done with spacers, whose thickness could be carefully adjusted, this would be true for it also. The net result is that the mechanical technique removes all defects except the oily streaks and it does not produce any other stable type of defect. Although the oily streaks can often be eliminated from the sample, this takes more care and patience than for other defects. Flow is observed during the mechanical process and this often eliminates defects.

The monodomain areas obtained by using the mechanical alignment technique are not as large in area as those obtained with the Powers thermal alignment technique (1–3). However, the sample thickness of mechanically aligned samples is almost as large (~100 μm). The monodomain areas in these mechanically aligned samples are defect-free and appear totally black between crossed polarizers. Although the samples contain some oily streaks, greater than 95% of a 1-cm^2 mechanically aligned sample is in the planar defect-free form. Typically, 3-mm^2 aligned domains can be prepared in a few hours at room temperature in 80-μm thick samples of DLPC containing 20% water. If the temperature of the lipid sample is increased, the mechanical alignment process proceeds more rapidly, obtaining larger aligned regions in shorter times. For example, 10-mm^2 areas can be prepared in ~1 h at 60°C in DLPC samples containing 20% water by weight.

DISCUSSION

Phosphatidylcholines are amphiphilic, due to their distinct polar and nonpolar parts (8). The hydrophobic hydrocarbon chains of these molecules associate together in the Lα liquid crystalline phase to form bimolecular leaflets, while the hydrophilic choline headgroups face out of the bilayer and are associated with the interleaved water layers (Fig. 2). In thermodynamic equilibrium, at a fixed water concentration, the repeat distance between the bilayers is fixed by thermal equilibrium conditions. In contact with a planar boundary of the type used in our experiments, the minimum free energy would be achieved for a perfectly aligned, homogeneous system, with the layers parallel to the glass slides. On the other hand, there is an extensive literature concerning the types of defects that are observed to exist in lamellar or smectic-A systems that are not in states of minimum free energy (36–42). Presumably, kinetic effects, impurities, pinning sites at the boundaries, or other subtler defect-defect interactions render the defects metastable.

Since the most stable defects should cause only small increases in the free energy over the planar configuration, the interplanar repeat distance should be approximately conserved and the layer curvature should be small throughout most of the sample (38). These criteria are closely approximated if the layers form a family of surfaces known as Dupin cyclides (36–42). Each of these surfaces curves smoothly while maintaining a constant layer repeat distance, except at a few isolated points in the surface where cusps occur. Mathematical theorems exist to prove that the lines forming the loci of these cusps occur as a confocal ellipse and hyperbola or some degenerate form of these, such as a circle and straight line pair (Fig. 15 *a*). In the latter case the smectic layers form toroids concentric with the circle. The cusps in the

curvature of the individual toroidal layers lie along a line perpendicular to the circle and passing through its center. A somewhat more complex and more common focal conic defect occurs when the circle becomes an ellipse and the line becomes a hyperbola passing through one of the foci of the ellipse (Fig. 15 *b*). Electron micrographs of lipid bilayer curvatures similar to those shown in Figs. 15 *a* and *b* were recently obtained by Kleman et al. (36).

These focal conic defects are observed in the optical microscope in lipid samples because of the refractive index discontinuities along the cusp lines (i.e., along the ellipse and hyperbola), and because the layer tilts around the defect modulate the sample birefringence. These particular defects have never been identified by us in pure lipid-water samples, but are seen in samples of DLPC-cholesterol and water (Fig. 15 *c*).

The focal conic shown in Fig. 15 *c* was photographed such that the focus of the microscope was at the center of ellipse. The hyperbola running between points *PP'* lies in the plane of the figure and is almost a straight line. The ellipse in the figure is somewhat out of focus, but if the focus of the microscope is changed it is very clear that an ellipse oriented almost edge on to the viewing plane is present.

Polygonal Arrays

A degenerate form of the focal conic defect results when the straight line and the circle are deformed into two confocal parabolas. Rosenblatt et al. (37) have demonstrated that in thermotropic smectic liquid crystals a network of parabolic focal conics (PFC's) is responsible for a defect structure that resembles the polygonal structure discussed above. In an earlier paper (7) we have demonstrated unambiguously that the simple PFC structure shown in Figs. 16 and 17 is responsible for the least birefringent polygonal structures observed in the lipids (Figs. 7 *a* and *b*).

Because the detailed properties of these arrays were described elsewhere (7), we will restrict the present discussion to some of their more important features. Fig. 16 illustrates an array of the confocal parabolas of a PFC array. As previously mentioned, the parabolic lines are the locus of cusps in the curvature of the individual smectic layers. Fig. 17 illustrates the layer curvatures at four different heights in the sample for one section of the array shown in Fig. 16. Near the cusps in layer 1 of Fig. 17 *a* the layers are all tilted towards the points marked A. Since the system is locally uniaxial with the symmetry axis normal to the layers, the sample, when viewed from above, will appear birefringent with the optic axis radiating out

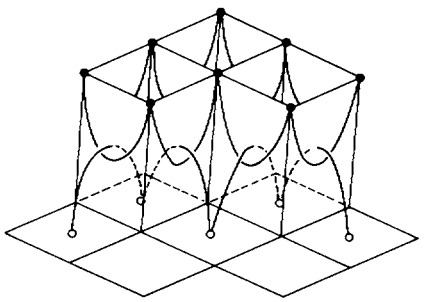

FIGURE 16 Three-dimensional structures of the locus of the cusps of the parabolic focal conics. (After Rosenblatt et al. [37].)

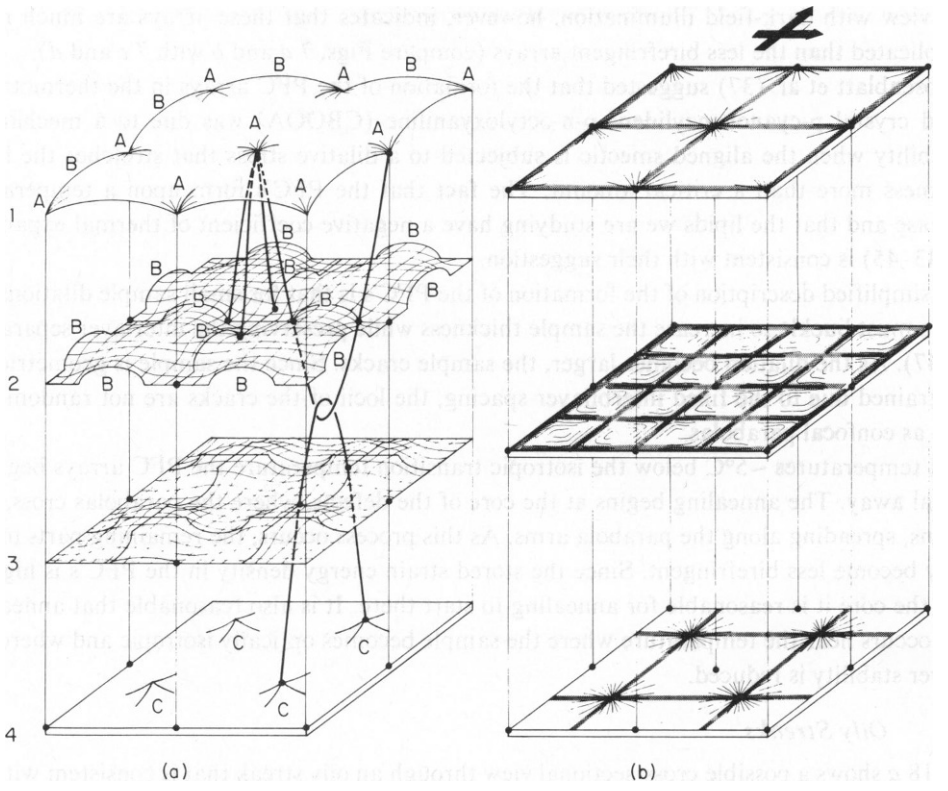

FIGURE 17 Representation of the smectic layer tilts in a PFC array and the effect of crossed polarizers. (*a*) Three-dimensional view of the layer tilts at four different heights in the sample. Points labeled A are where the four parabolas join at the top. Points labeled B are where the parabolas cross. Points labeled C are where the four parabolas join at the bottom. (*b*) Locus of extinguished light by the crossed polarizers oriented along the parabola.

from point A. The projection of the optic axes on the viewing plane is shown by the fine lines in Fig. 17 *b*. Thus, if this layer were isolated and viewed between crossed polarizers oriented as indicated above Fig. 17 *b*, one should see the square network shown by the heavy lines. In fact, if the sample is viewed with a microscope that has a short depth of focus and that is focused at this sample height, the predicted pattern is just this (7). Similar effects are expected if the microscope is focused at the bottom layer, except that the bottom network is displaced relative to the top network. Focusing at the midheight results in a square network of half the spacing (7).

The largest layer tilts occur where the two parabolas wrap around one another in the midheight of the figure (and in the sample also). These large tilts and the refractive index inhomogeneities they create are responsible for the fine light crosses seen in the dark-field microscopic view shown in Fig. 7 *b*.

The more birefringent arrays shown in Fig. 7 *c* and seen in Fig. 6 appear slightly different from the others when viewed between crossed polarizers. Faint, additional structure can be seen in the interior of the square arrays. Also, when viewed with white light, but between crossed polarizers, these arrays are colored while the initial, less birefringent arrays are not.

The view with dark-field illumination, however, indicates that these arrays are much more complicated than the less birefringent arrays (compare Figs. 7 *a* and *b* with 7 *c* and *d*).

Rosenblatt et al. (37) suggested that the formation of the PFC arrays in the thermotropic liquid crystal p-cyanobenzylidene-p-n-octyloxyaniline (CBOOA) was due to a mechanical instability when the aligned smectic is subjected to a dilative stress that stretches the layer thickness more than a critical amount. The fact that the PFC's form upon a temperature increase and that the lipids we are studying have a negative coefficient of thermal expansion (25,43–45) is consistent with their suggestion.

A simplified description of the formation of the PFC's is that for small sample dilations the layers must buckle to increase the sample thickness while preserving the interlayer separation (46,47). As the dilation becomes larger, the sample cracks. Since the sample is geometrically constrained due to the fixed interbilayer spacing, the locii of the cracks are not random and form as confocal parabolas.

At temperatures ~5°C below the isotropic transition temperature the PFC arrays begin to anneal away. The annealing begins at the core of the defects, where the parabolas cross, and widens, spreading along the parabola arms. As this process occurs, the remaining parts of the array become less birefringent. Since the stored strain energy density in the PFC's is highest near the core it is reasonable for annealing to start there. It is also reasonable that annealing only occurs near the temperature where the sample becomes optically isotropic and where the bilayer stability is reduced.

Oily Streaks

Fig. 18 *a* shows a possible cross-sectional view through an oily streak that is consistent with all of the above observations. This structure could be viewed as two equal and opposite dislocations with large Burgers vectors. In the figure the Burgers vectors are equal to 11 lattice vectors, but in some of the oily streaks ~5 μm wide the Burgers vector would have to be of the order of 10^3 lattice spacings and it is not clear that it is profitable to speak of a defect of this size as a dislocation. The proposed structure differs from the focal conic defects in that for each layer, the singularity in curvature is a line rather than a point, and the locus of singularities is a plane rather than a line. If the focal conic defect is considered to be a line or a one-dimensional defect, we are proposing that the oily streak is a planar or two-dimensional defect.

The evidence supporting this structure is as follows: firstly, as indicated in Results, the layers are tilted such that the layer normals remain perpendicular to the long axis of the oily streak. Secondly, the phase shift or optical path difference between two vertical rays, one polarized parallel to the axis of the streak and the other perpendicular, is predicted from this model to vary across the width of the streak. If we express the phase shift as an optical path difference, Δd, it is straightforward to demonstrate that for the path PP' shown in Fig. 18 *a*,

$$\Delta d = 2\Delta n x \tan^{-1} \frac{t}{2x},$$

where Δn is the difference in index of refraction between light polarized along the uniaxial direction and perpendicular to that axis, and t is the "effective height" of the sample. Although the full height of the sample is 125 μm, our observations indicate that none of the

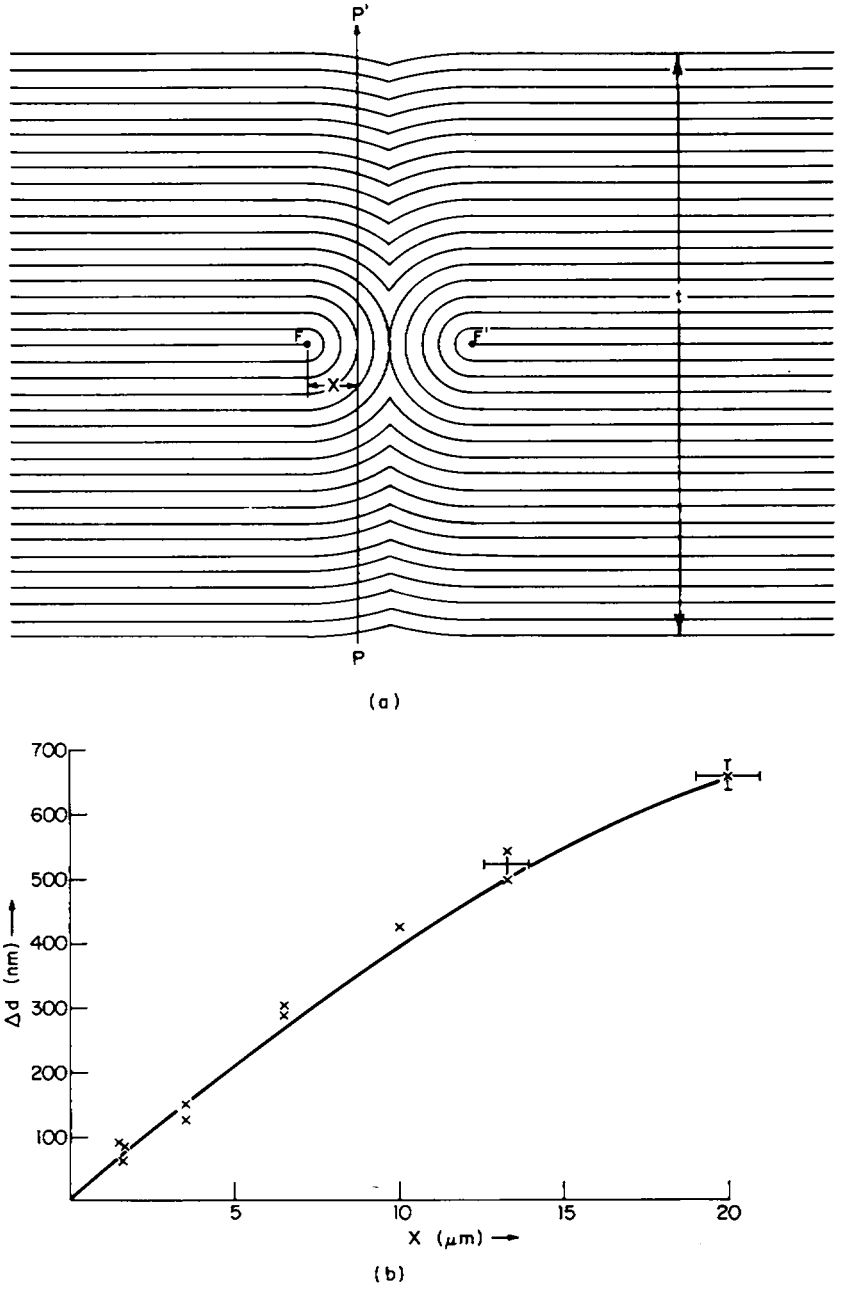

FIGURE 18 (*a*) Proposed structure for oily streaks showing layer curvatures. (*b*) Measured birefringence as a function of x across half of an oily streak 40 μm wide in a 125-μm sample of DPPC with 7% water. The birefringence is symmetric with respect to the long axis of the streak. T = 90°C. Δd is optical path difference in nanometers. Solid line is the calculated Δd for $\Delta n = 0.015$ and $t = 80$ μm.

oily streaks contact the surface except at nodes where the oily streaks join. Previously, we drew the same conclusions from studies of the PFC arrays (7). This suggests that the layers close to the surfaces are not readily deformable. Fig. 18 *b* compares the phase shift across an oily streak measured with a Soleil-Babinet compensator with values obtained from this formula using $\Delta n = 0.015$ and $t = 80\ \mu m$. The agreement is satisfactory given the fact that the model completely neglects the small but finite compressibility of the layers and the small but finite elastic resistance to layer curvature. Both of these should induce small deviations between the layer tilts in Fig. 18 *a* and the true values. Additional layers might also exist along the disclination plane to alleviate the larger layer curvatures. Thirdly, the black lines observed in the PFC structures for suitable orientations of the polarizer and analyzer were observed to continue into the oily streak (Fig. 6). This is consistent with the proposed structure, since the middle of the oily streak consists of only a thin disclination line near the midheight of the streak. Above and below this disclination the sample is essentially planar and there is no reason why the focal conic lines that make up the PFC array should not extend into this part of the sample. The transverse lines do not appear to continue through the oily streak. Instead, they curve, and a zigzag pattern is observed, often centered along the middle of the streak. The complicated pattern of dark zigzagging lines transverse to the streak changes as the focus is shifted; other zigzag patterns emerge at different heights. Although we do not have a model for this complicated pattern, the model we propose for the oily streaks is sufficiently well-ordered so that one expects focal conic-like defects to exist in the streak itself. These lines, interacting with the disclination line that forms the core of the streak, could themselves form new conjugate focal curves.

Fourthly, it is energetically unfavorable for impurities such as dust and insoluble materials to exist in planar regions of the sample and these materials would be expected to be expelled out of the aligned regions (35). In the first instance they could very well become trapped along the highly strained core regions of the oily streak. However, since the streak is itself well-ordered along its length, it is not surprising that the impurities would migrate along the streak, eventually becoming located at the nodes. Fifthly, it is easy to visualize that several oily streaks may be located alongside each other and that transverse flow patterns could supply the forces necessary to separate them. Variations on the simple model are also not ruled out. For example, the two cores may not always be at the same height, or one may find an oily streak consisting of one large Burgers vector matched with two or more smaller ones of opposite sign.

Finally, it is well known that Kirchhoff networks are essential features of dislocations and, as Kleman et al. (6) pointed out, these are characteristic of the oily streaks we observe.

Ring Defects

The ring defects that are shown in Figs. 13 and 14 only appear within ~5° of the transition to the isotropic phase and do not last long enough to allow careful study. Nevertheless, their properties, when viewed between crossed polarizers, indicate that the smectic layer normals are perpendicular to the light and dark bands. Also, the observation that the pattern seen when the microscope is focused on the top of the sample (Fig. 14 *a*) is the precise complement of the one seen when focused on the bottom (Fig. 14 *b*) suggests some sort of staggered structure. Structures such as "William's domains" (48) that might appear similar to this have previously been observed in liquid crystals. However, these have all been interpreted in terms

of lens effects in which the light is brought to different focii by index of refraction gradients in the sample. For lipids the refractive index gradients are an order of magnitude smaller than those in thermotropic liquid crystals and the same interpretation is not possible.

Fig. 19 *a* schematically describes the layer curvatures for one structure that could be responsible for the observations. Since the bilayers are locally uniaxial, the bilayer tilts are accompanied by refractive index inhomogeneities. Fig. 19 *b* illustrates the difference Δn_{eff} between the indices of refraction for light propagating normal to the glass and polarized parallel and perpendicular to the plane of the figure. The three curves indicate the spatial behavior for Δn_{eff} at the top, middle, and bottom of the sample. Light that is polarized neither parallel nor perpendicular to the plane of the figure will become elliptically polarized after traversing the sample. If the microscope were focused at points A at the top (or bottom) of the sample, the acceptance angle of the microscope objective would allow the cones of light enclosed by the triangular sections 1 (or 2) to be sampled. Since the light rays within these cones traverse sections containing only small layer tilts, the light remains largely linearly polarized and can be extinguished by a crossed polarizer, rendering points A at the top (and bottom) of the sample dark. However, if the focus occurs at other points in the sample, the acceptance cone lies in more strongly tilted regions of the sample and the light becomes elliptically polarized and is partially transmitted through the crossed polarizer (see sections 3–5 in Fig. 19 *b*), rendering the sample bright. Thus, a staggered pattern of light and dark occurs when the microscope is focused at the top and bottom of the sample. The widths of the black areas should be smaller than those of the light areas.

The concentric ring patterns observed in Figs. 13 and 14 can be explained if the structure in Fig. 19 *a* had a rotation axis along the line marked *P*. A series of concentric light and dark rings would appear with the dark rings at the bottom surface occurring in the center of the light rings observed at the top and vice versa.

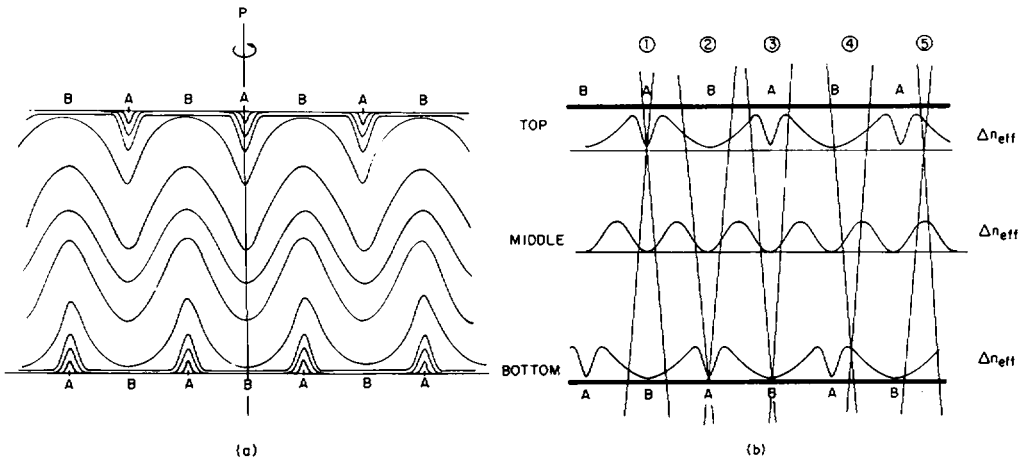

FIGURE 19 (*a*) Possible structure for the ring defects shown in Figs. 13 and 14. The lines represent average layers curvatures and not individual layers. (*b*) Qualitative representation of the variation of Δn_{eff} as a function of position and height in the sample for the defect structure shown in (*a*). The numbered segments enclosed by intersecting lines represent various cones of light rays accepted by the microscope objective. See text for further details.

The projection of the local optic axes of the defect on the viewing plane would be everywhere radial; light would be extinguished in the light bands along lines oriented along the polarizer axes. Thus, a large dark cross would be observed centered at P and would rotate as the crossed polarizers were rotated with respect to the sample.

Relationship between Defect Structures and Lipid Phases

We have observed that the PFC's and the oily streaks are defect textures characteristic of the Lα phase of lipids. The PFC's result from small elastic strains on planar aligned domains. The origin of the oily streaks is less clear. However, large strains occurring within the Lα phase can form defects similar to the oily streaks (Fig. 10), suggesting that they may result from the large sample strains that occur during the $L_{\beta'}$ to Lα transition (24,28). The oily streaks could also result from other factors, such as molecular packing in the samples below the Lα phase or water concentration inhomogeneities.

The structure we propose for the ring defects assumes a layered geometry similar to that in the Lα phase. However, we cannot neglect the possibility that this new texture could be due to the presence of an additional phase confined to a narrow temperature region between the Lα and the isotropic phase. This phase would be uniaxial with a small refractive index anisotropy and could be hexagonal or rhombohedral (29). However, we cannot detect any border between sample domains that support PFC's and those domains that support ring defects. In contrast, a clear border is observed by using unpolarized light between ring defect regions and optically-isotropic lipid domains. The evolution of the ring defect texture with increasing temperature from an angular polygonal texture reminiscent of PFC's to a smooth ring texture may indicate that the ring texture originates from pretransitional effects near the phase transition from the Lα phase to an optically isotropic phase, which we presume is cubic in nature. The smectic elastic constants would change near the transition and possibly permit this new defect. Alternatively, the domains supporting the ringed defects may be regions where microscopic domains of the Lα and optically isotropic phase coexist.

Steam formation in Lipid-Water Samples

Although published phase diagrams of hydrated lecithins indicate that the Lα phase can absorb up to 40% water by weight for all temperatures at which the Lα phase is stable (8,22,23), the experimental data we are aware of only documents this for temperatures below 100°C. Presumably at 40% by weight the chemical potential for water within the lipid phase is equal to that of bulk water and the two systems coexist in thermal equilbrium. The fact that the phase boundary remains at 40% for all temperatures below 100°C suggests that at maximum hydration the water within the Lα phase is not very different from bulk water. In contrast, our observation of steam formation in lipid samples containing as little as 10% water by weight demonstrates that for atmospheric pressure and 120°C the condition for maximum hydration is determined by coexistence of the lipid with water vapor rather than with liquid water.

Since the water between the lipid bilayers at 40% water by weight is probably very much like liquid water (8,23,49,50) and since the vapor pressure of liquid water is above 1 atm when the temperature exceeds 100°C, the vapor pressure of water in the lipid samples that contain 40% water will also be above 1 atm for $T > 100$°C. Because both the chemical potential and

the vapor pressure of water in the lipid are monotonically increasing functions of water content, if the water vapor pressure of a lipid water sample is maintained at 1 atm, equilibrium between the water in the lipid and water vapor demands that the water concentration in the lipid will have to decrease for temperatures above 100°C. If we assume that the gas bubbles observed at 120°C in samples containing 10% water by weight correspond to water vapor at 1 atm, we can estimate the difference between the chemical potential of water in lipid samples containing 40 and 10% water by weight at 120°C from $\Delta\mu = -RT \ln P_s/P_L$, where P_s is the saturated vapor pressure of steam at 120°C (51) and P_L = 1 atm; $\Delta\mu = -523$ cal/mol. Using Elworthy's (49,50) results for the partial pressure of water over DPPC samples containing 10% water by weight, we obtain $\Delta\mu = -316$ cal/mol at 40°C. The agreement is surprisingly good in view of the crude assumptions we have used, especially since P_L must be >1 atm to force the lipid out of our sample holders. In fact, if $\Delta\mu = -316$ cal/mol at 120°C, the partial pressure of water would be 1.3 atm.

Although Small (23) interpreted his results so as to make a distinction between free water (above 16%) and bound water (below 16%), more recent studies (10,52) demonstrate that there is not a clear distinction between the two. The greatest changes in the chemical potential for water occur for lower concentrations and the value of $\Delta\mu$ that we calculate is only a small fraction of the binding energy of the first few percent of water that is added to the anhydrous system.

The appearance of an additional water vapor phase at atmospheric pressure and at temperatures above 100°C is not reflected in any of the published phase diagrams we are aware of. This means that at high temperatures sealed samples with small free volumes cannot be treated as though they were at constant pressure and samples with large free volumes are probably not adequately treated by assuming fixed water content.

CONCLUSIONS

Numerous defect structures are observed and characterized in these lipid liquid crystals. All of these can be annealed out at temperatures close to the smectic-isotropic transition. However, if the entire sample is taken into the isotropic phase, a set of defects appears that does not anneal away. Care must be taken in aligning these systems at elevated temperatures to avoid thermal decomposition of the lipid; to maintain high purity aligned samples the high temperature annealing process must be as brief as possible. A mechanical alignment technique is discussed that avoids thermal decomposition by facilitating sample alignment at lower temperatures than the Powers technique. Lipid samples containing >8% water by weight cannot be thermally annealed into aligned samples due to steam formation that disrupts the sample. However, these samples can be aligned by the mechanical alignment technique. The observations of steam formation in samples with water concentrations as low as 10% by weight at temperatures >120°C indicates the coexistence of both a lipid-water and water vapor phase above ~120°C. This fact is not reflected in any of the published phase diagrams that we are aware of.

We would like to gratefully acknowledge helpful conversations and criticisms from Robert Meyer, Michael Fisch, Jeff Collett, and Marc Peterson. We would also like to acknowledge Mr. Paul Demchak for technical assistance in the early stages of this work and thank Jeff Collett for assistance in some of the measurements.

This work has been sponsored in part by the Joint Services Electronics Program (U.S. Army, Navy, and Air Force) under contract N00014-75-C-0648, by the National Science Foundation under grant DMR-76-01111, and by the National Institutes of Health under grant GM-24081-01.

Received for publication 18 December 1978 and in revised form 26 March 1979.

REFERENCES

1. POWERS, L., and P. S. PERSHAN. 1977. Monodomain samples of dipalmitoylphosphatidylcholine with varying concentrations of water and other ingredients. *Biophys. J.* **20**:137–152.
2. POWERS, L., and N. A. CLARK. 1975. Preparation of large monodomain phospholipid bilayer smectic liquid crystals. *Proc. Natl. Acad. Sci. U.S.A.* **72**:840–843.
3. POWERS, L. 1976. Preparation and investigation of monodomain phospholipid bilayer-water systems. Ph.D. Thesis. Harvard University, Cambridge, Mass.
4. MICCIANCIO, S., and F. RONDELEZ. 1978. Evidence for shear-induced biaxiality in Lα lecithins close to solid surfaces. *J. Phys. (Paris) Lett.* L-5-9.
5. BROCHARD, F., and P. G. DEGENNES. 1975. Hydrodynamic properties of fluid lamellar phases of lipid/water. *Pramana.* Suppl. 1, 1–21.
6. KLEMAN, M., C. COLLIEX, and M. VEYSSIE. 1976. Recognition of defects in water-lecithin Lα phases. *Adv. Chem. Ser.* **152**:71–84.
7. ASHER, S. A., and P. S. PERSHAN. 1979. Parabolic focal conics and polygonal textures in lipid-liquid crystals. *J. Phys. (Paris).* **40**:161–173.
8. CHAPMAN, D. 1975. Phase transitions and fluidity characteristics of lipids and cell membranes. *Q. Rev. Biophys.* **8**:185–235.
9. MELCHIOR, D. L., and J. M. STEIN. 1976. Thermotropic transitions in biomembranes. *Annu. Rev. Biophys. Bioeng.* **5**:205–238.
10. CHAN, W. K., and P. S. PERSHAN. 1978. Water and thermal diffusivity in a lipid-water smectic phase. *Biophys. J.* **23**:427–449.
11. SMITH, B. A., and H. M. MCCONNELL. 1978. Determination of molecular motion in membranes using periodic pattern photobleaching. *Proc. Natl. Acad. Sci. U.S.A.* **75**:2759–2763.
12. LEPESANT, J-P., L. POWERS, and P. S. PERSHAN. 1978. Brillouin light scattering measurements of the elastic properties of aligned multilamella lipid samples. *Proc. Natl. Acad. Sci. U.S.A.* **75**:1792–1795.
13. CHAN, W., and P. S. PERSHAN. 1977. Forced Rayleigh scattering from lipid-water smectic phases. *Phys. Rev. Lett.* **39**:1368–1371.
14. WU, E-S., K. JACOBSON, and D. PAPAHADJOPOULOS. 1977. Lateral diffusion in phospholipid multilayers measured by fluorescence recovery after photobleaching. *Biochemistry.* **16**:3936-3941.
15. JOST, P., L. J. LIBERTINI, V. C. HEBERT, and O. H. GRIFFITH. 1971. Lipid spin labels in lecithin multilayers. A study of motion along fatty acid chains. *J. Mol. Biol.* **59**:77–98.
16. LEVINE, Y. K., and M. H. F. WILKINS. 1971. Structure of oriented lipid bilayers, *Nat. New Biol.* **230**:69–72.
17. HSIA, J-C., H. SCHNEIDER, and I. C. P. SMITH. 1970. Spin label studies of oriented phospholipids: egg lecithin. *Biochim. Biophys. Acta.* **202**:399–402.
18. SEELIG, J. 1970. Spin label studies of oriented liquid crystals (a model system for bilayer membranes). *J. Am. Chem. Soc.* **92**:3881–3887.
19. LIBERTINI, L. J., A. S. WAGGONER, P. C. JOST, and O. H. GRIFFITH. 1969. Orientation of lipid spin labels in lecithin multilayers, *Proc. Natl. Acad. Sci. U. S. A.* **64**:13–19.
20. LEVINE, Y. K., A. I. BAILEY, and M. H. F. WILKINS. 1968. Multilayers of phospholipid bimolecular leaflets, *Nature (Lond.).* **220**:577–578.
21. ELWORTHY, P. H. 1959. The structure of lecithin micelles in benzene solution *J. Chem Soc. (Lond.).* 1951–1956.
22. CHAPMAN, D., R. M. WILLIAMS, and B. D. LADBROOKE. 1967. Physical studies of phospholipids. VI. Thermotropic and lyotropic mesomorphism of some 1,2-diacyl-phosphatidylcholines (lecithins), *Chem. Phys. Lipids.* **1**:445–475.
23. SMALL, D. M. 1967. Phase equilibria and structure of dry and hydrated egg lecithin, *J. Lipid Res.* **8**:551–557.
24. WILLIAMS, R. M., and D. CHAPMAN. 1970. Phospholipids, liquid crystals and cell membranes, *Prog. Chem. Fats Other Lipids.* **11**:1–79.
25. LUZZATI, V. 1968. X-ray diffraction studies of lipid-water systems in biological membranes, *In Biological Membranes.* D. Chapman, editor. Academic Press, Inc., New York. 71.

26. LUZZATI, V., and A. TARDIEU. 1974. Lipid phases: Structures and structural transitions. *Annu. Rev. Phys. Chem.* **25**:79–94.
27. JANIAK, M. J., D. M. SMALL, and G. G. SHIPLEY. 1976. Nature of the thermal pretransition of synthetic phospholipids, dimyristoyl and dipalmitoyl-lecithin. *Biochemistry.* **15**:4575.
28. TARDIEU, A., V. LUZZATI, and F. C. REMAN. 1973. Structure and polymorphism of the hydrocarbon chains of lipids: A study of lecithin-water phases. *J. Mol. Biol.* **75**:711–733.
29. LUZZATI, V., T. GULIK-KRZYWICKI, and A. TARDIEU. 1968. Polymorphism of lecithins. *Nature (Lond.).* **218**:1031–1034.
30. LOOMIS, C. R., M. J. JANIAK, D. M. SMALL, and G. G. SHIPLEY. 1974. The binary phase diagram of lecithin and cholesteryl linolenate. *J. Mol. Biol.* **86**:309–324.
31. LENTZ, B. R., E. FREIRE, and R. L. BILTONEN. 1978. Fluorescence and calorimetric studies of phase transitions in phosphatidylcholine multilayers: Kinetics of the pretransition. *Biochemistry.* **17**:4475–4480.
32. LUZZATI, V., and P. A. SPEGT. 1967. Polymorphism of lipids. *Nature (Lond.).* **215**:701–704.
33. LUZZATI, V., A. TARDIEU, T. GULIK-KRZYWICKI. 1968. Polymorphism of lipids. *Nature (Lond.).* **217**:1028–1031.
34. ROSEVEAR, F. B. 1954. The microscopy of the liquid crystalline neat and middle phases of soaps and synthetic detergents. *J. Am. Oil Chem. Soc.* **31**:628–638.
35. PERSHAN, P. S., and J. PROST. 1975. Dislocation and impurity effects in smectic-A liquid crystals. *J. Appl. Phys.* **46**:2343–2353.
36. KLEMAN, M., C. E. WILLIAMS, M. J. COSTELLO, and T. GULIK-KRZYWICKI. 1977. Defect structures in lyotropic smectic phases revealed by freeze-fracture electron microscopy. *Phil. Mag.* **35**:33–56.
37. ROSENBLATT, C. S., R. PINDAK, N. A. CLARK, and R. B. MEYER. 1977. The parabolic focal conic: A new smectic A defect. *J. Phys. (Paris).* **38**:1105–1115.
38. KLEMAN, M. 1976. Remarks on a possible elasticity of membranes and lamellar media: disordered layers. *Proc. Roy. Soc. Lond. A. Math. Phys. Sci.* **347**:387–404.
39. KLEMAN, M. 1977. Energetics of the focal conics of smectic phases. *J. Phys. (Paris).* **38**:1511–1518.
40. BOULIGAND, Y. 1972. Réchérches sur les textures des êtats mésomorphes 1. Les arrangements focaux dans le smectiques: rappels et considerations théoretiques. *J. Phys. (Paris).* **33**: 525–547.
41. BRAGG, W. H. 1934. Liquid crystals. *Nature (Lond.).* **133**:445–456.
42. FRIEDEL, G. M. 1922. Les états mesomorphes de la matière. *Ann. Phys.* **18**:273.
43. RAND, R. P., and W. A. PANGBORN. 1973. A structural transition in egg lecithin-cholesterol bilayers at 12°C. *Biochim. Biophys. Acta.* **318**:299–305.
44. RANCK, J. L., L. MATEY, D. M. SADLER, A. TARDIEU, T. GULIK-KRZYWICKI, and V. LUZZATI. 1974. Order-disorder conformational transitions of the hydrocarbon chains of lipids. *J. Mol. Biol.* **85**:249–277.
45. LUZZATI, V., H. MUSTACCHI, A. STOULIOS, and F. JUSSON. 1960. La structure des colloides d'association. I. Les phases liquidecristallines des systèmes-êau, *Acta Crystallogr.* **13**:660–677.
46. CLARK, N. A., and R. B. MEYER. 1973. Strain induced instability of monodomain smectic A and cholesteric liquid crystals. *Appl. Phys. Lett.* **22**:493–494.
47. DELAYE, M., R. RIBOTTA, and G. DURAND. 1973. Buckling instability of the layers in a smetic-A liquid crystal. *Phys. Lett.* **44A**:139–140.
48. DEGENNES, P. B. 1974. The Physics of Liquid Crystals, Oxford University Press, London, 196.
49. ELWORTHY, P. H. 1961. The absorption of water vapor by lecithin and lysolecithin, and the hydration of lysolecithin micelles. *J. Chem. Soc.* **00**:5385–5389.
50. ELWORTHY, P. H. 1962. Sorption studies on phosphatides. Part II. Sorption of water vapor by a synthetic lecithin and cephalin. *J. Chem. Soc. (Lond.).* **00**:4879–4900.
51. Handbook of Chemistry and Physics. Chemical Rubber Co., Cleveland. Vol. 45. E9.
52. LENEVEU, D. M., R. P. RAND, V. A. PARSEGIAN, and D. GINGELL. 1977. Measurement and modification of forces between lecithin bilayers. *Biophys. J.* **18**:209–230.